Materials Advances

ROYAL SOCIETY OF CHEMISTRY

PAPER

Quinoline-tagged fluorescent organic probes for sensing of nitro-phenolic compounds and Zn²⁺ ions at the ppb level†

Gouri Chakraborty, Prasenjit Das and Sanjay K. Mandal (ID) *

With variation in the spacer from flexible tetra-methylene to semi-rigid xylylene, connecting quinoline chromophores and Lewis basic pyridyl groups on both ends, two new fluorescent sensors, N,N'-bis(pyridin-2-ylmethyl)-N,N'-bis(quinolin-2-ylmethyl)butane-1,4-diamine (**bqbpbn**, **1**) and N,N'-(1,4-phenylenebis(methylene))-bis(1-(pyridin-2-yl)-N-(quinolin-2-ylmethyl)methanamine) (**bqbpxn**, **2**) have been designed and synthesised *via* simple reduced Schiff base chemistry followed by the nucleophilic substitution reaction under basic conditions in good yields. These were characterized by various analytical techniques, such as FT-IR, UV-vis and NMR (¹H and ¹³C) spectroscopy, and high resolution mass spectrometry (HRMS). The effect due to the change in the spacer was investigated towards the sensing of nitro-phenolic compounds, especially highly explosive 2,4,6-trinitrophenol (TNP) in water with a detection limit of 1.2 ppm and 0.3 ppm in **1** and **2**, respectively. The detailed mechanistic studies indicate that photo-induced electron transfer is more dominant in **2** due to the semi-rigid xylylene spacer favouring better detection of TNP. Both are potential for on-site TNP detection for practical applications. For this kind of application, the chemical and hydrolytic stability of **1** and **2** were established by powder X-ray diffraction (PXRD) and field-emission scanning electron microscopy (FESEM). The effect of flexible and semi-rigid spacers in these organic probes was further established by metal ion sensing, where **1** and **2** displayed selective sensing of Zn²⁺ (with the detection limit of 5 and 10 ppb, respectively) *via* chelation-enhanced fluorescence in aqueous medium with the formation of 1:1 and 1:2 adducts, respectively.

Introduction

In recent years, the design and development of potential single-molecule sensors has been a key research activity for the detection of lethal nitro-aromatic compounds (NACs) owing to their explosive nature, frequent use in military and mining applications and exploitation by terrorists.[1–5] This is directly affecting national/international security and the environment due to their destructive properties.[6,7] Among the various NACs including 2,4,6-trinitrophenol (TNP), 2,4,6-trinitrotoluene (TNT), 2,6-dinitrotoluene (2,6-DNT), 2,4-dinitrotoluene (2,4-DNT), 1,3,5-trinitro-1,3,5-triazacyclohexane (RDX), 1,3-dinitrobenzene (1,3-DNB) and nitrobenzene (NB), TNP and TNT are widely used in improvised explosive devices.[8,9] TNP has more explosive power than TNT and its different salts such as explosive D and pentolite

Department of Chemical Sciences, Indian Institute of Science Education and Research Mohali, Sector 81, Manauli PO, S.A.S. Nagar, Mohali, Punjab, 140306, India. E-mail: sanjaymandal@iisermohali.ac.in

† Electronic supplementary information (ESI) available: Characterization, experimental details of fluorescence and absorption spectroscopy, detection limit calculations, lifetime data and DFT calculations. See DOI: 10.1039/d1ma00025j

are the key ingredients for explosive formulations.[10–13] It is also used in industries for the synthesis of dyes, plastics, leather, fireworks *etc.* Due to its excessive use in various industries, there is an injudicious release to the environment causing several health hazards and detrimental impacts.[6,12] Furthermore, TNP is highly soluble in water leading to easy accumulation in the soil and groundwater, consequently affecting the aquatic system and environment.[14,15] Therefore, selective and sensitive detection of TNP in aqueous medium is strongly required.

Several fluorescent materials such as conjugated polymers,[16–18] macromolecules,[19] carbon dots,[20,21] small organic probes,[22–33] cages,[34,35] covalent organic frameworks[36–39] and metal–organic frameworks[40–50] have been utilized for TNP and small molecule detection. Most of these demonstrated TNP sensing in dichloromethane (DCM), dimethylformamide (DMF), tetrahydrofuran (THF) and other organic and aqueous-organic solvents,[16–19,33–40,42,43] however, for practical usage detection in water is highly in demand.[20,21,27–31,44–51] Thus, efforts are still required in developing fluorescent materials with high stability in water for this detection purpose. Various analytical techniques such as surface-enhanced Raman spectroscopy, mass spectrometry,

gas chromatography, cyclic voltammetry and fluorescence spectroscopy have been employed for TNP detection out of which fluorescence based sensing has gained more attention due to cost-effectiveness, high sensitivity, real-time detection and rapid response time.[52–61] The detection of electron-deficient NACs is based on different signaling mechanisms, *e.g.*, resonance energy transfer (RET), photoinduced electron transfer (PET), inner filter effect (IFE), intramolecular charge transfer (ICT) and electrostatic interactions. Depending upon the interaction site present in the sensor, detection can be based on the above-mentioned interactions. Recently, we have reported two fluorescent sensors based on naphthalene and anthracene fused rings along with pyridyl moieties connected by a tetra-methylene spacer and demonstrated their role in TNP detection.[62] This study provided a platform to design different fluorescent sensors with some variation and increase the sensing capabilities towards TNP.

With the consideration of all the above-mentioned factors, we have designed and synthesized two fluorescent sensors, *N,N′*-bis(pyridin-2-ylmethyl)-*N,N′*-bis(quinolin-2-ylmethyl) butane-1,4-diamine (**bqbpbn**, **1**) and *N,N′*-(1,4-phenylenebis (methylene))bis(1-(pyridin-2-yl)-*N*-(quinolin-2-ylmethyl)methanamine) (**bqbpxn**, **2**), based on quinoline and pyridine moieties with a variation in spacer from flexible tetra-methylene in **1** to semi-rigid xylylene in **2**, under ambient reaction conditions (Scheme 1). In the design of these two sensors, different moieties have the following roles: (i) quinoline is the source of fluorescence that can provide π–π interaction with the NACs and the nitrogen atoms can be involved in electron transfer or H-bonding interactions with the acidic phenolic NACs, (ii) Lewis basic pyridyl groups similar to quinoline can act as a recognition site *via* H-bonding, and (iii) the xylylene spacer in **2** can participate in further π–π interaction *via* electron transfer or energy transfer with the suitable NACs, which is not possible in **1** due to the presence of the tetra-methylene spacer. Although several quinoline based sensors are reported in the literature for metal ion sensing,[63–69] the same for the detection

of TNP is very rare.[70] Furthermore, the effect on the detection of TNP by the variation in spacer has not been studied so far. Herein, we report the synthesis and characterization of **1** and **2** and sensing of TNP in water with the detection limit of 1.2 ppm and 0.3 ppm by **1** and **2**, respectively, due to the variation in the spacer. Furthermore, **1** and **2** displayed enhancement in fluorescence intensity due to the Zn^{2+} ion among many other metal ions in 1:1 and 1:2 ratios, respectively, showing the effect of flexible tetra-methylene and semi-rigid xylylene spacers.

Experimental section

Materials and methods

All chemicals and solvents were commercially purchased and used as received without further purification.

CAUTION! Highly explosive TNP and TNT should be handled carefully in dilute solutions and in small amounts with safety measures in place to avoid an explosion.

Physical measurements

FT-IR spectra of **1** and **2** were recorded as KBr pellets in the 4000–400 cm^{-1} range on a PerkinElmer Spectrum I spectrometer. The ^1H and ^{13}C NMR spectra of **1** and **2** ligands were obtained in $CDCl_3$ solution at 25 °C on a Bruker ARX-400 spectrometer. Chemical shifts are reported relative to the residual solvent signals. Melting points were determined by a Büchii M-565 instrument with a heating rate of 10 °C per minute. The solution-state UV-vis spectra of NACs were recorded on an Agilent Cary 5000 spectrometer. The solid-state diffuse-reflectance spectra of probes were recorded on an Agilent Cary 5000 spectrometer with an integrating sphere attachment. High resolution mass spectrometry (HRMS) was performed using a Thermo Scientific LTQ XL LC-MS instrument for the 50–2000 amu range with ESI ion source. PXRD data were recorded on a Rigaku Ultima IV diffractometer equipped with 3 kW sealed-tube Cu Kα X-ray radiation (generator power settings: 40 kV and 40 mA) and a DTex Ultra detector using the BB geometry over the angle range 5–50° with a scanning speed of 2° min^{-1} with a 0.02° step. Fluorescence spectra were recorded using a Horiba Jobin-Yvon Fluorolog 3 Spectrophotometer with stirring attachment. The quantum yields of **1** and **2** were determined by using the following equation: $\varphi_s = \varphi_r (OD_r/OD_s) (I_s/I_r) (n_s^2/n_r^2)$, where φ_s and φ_r are quantum yields of **1** or **2** and the reference, respectively, OD is the optical density, I is the area under the curve for the emission spectra and n is the refractive index of the medium; the quinine sulfate ($\varphi_r = 0.546$, 0.1 M H_2SO_4) was used as the reference. Lifetime decay profiles of **1** and **2** were carried out using the time resolved Horiba Scientific Single Photon Counting Controller. The surface morphology of the as-prepared samples was examined using field-emission scanning electron microscopy (FESEM, JEOL, 8 or 15 kV).

Synthesis of *N,N′*-bis(quinolin-2-ylmethyl)butane-1,4-diamine (H₂bqbn)

In a 10 mL round-bottom (RB) flask, a solution of 2-quinoline carboxaldehyde (314 mg, 2 mmol) prepared in 6 mL CH_3OH
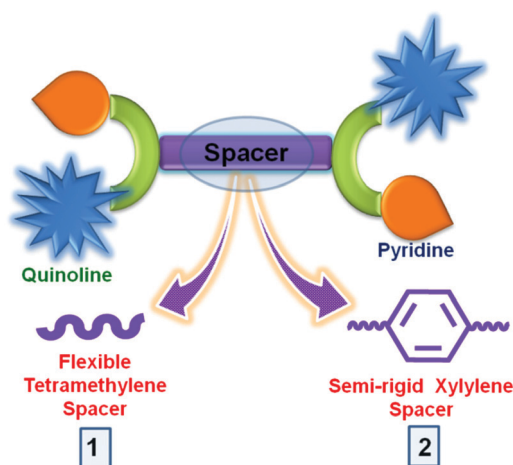
Scheme 1 Schematic representation of **1** and **2** showing the difference of the spacer.

was taken. To the above solution, a methanolic solution of 1,4-diaminobutane (0.1 mL, 1 mmol in 1 mL methanol) was added dropwise with continuous stirring. Then, an excess of NaBH$_4$ (3 equiv., 114 mg) was added step wise at 0 °C and stirred for 24 h at 30 °C to obtain a clear light yellow solution. The solvent was removed under reduced pressure to obtain a solid residue which was washed with water and extracted with chloroform. The organic layer was dried with anhydrous Na$_2$SO$_4$ and filtered followed by evaporation of solvent to get a pale yellow solid. Yield: 278 mg (75%). M.P. 90–93 °C. ^{1}H NMR (400 MHz, CDCl$_3$): δ 1.67 (t, 4H), 2.76 (t, 2H), 4.11 (s, 4H), 7.46 (d, J = 8.4 Hz, 2H), 7.52–7.70 (m, 4H), 7.81 (d, J = 8.0 Hz, 2H), 8.05 (d, J = 8.4 Hz, 2H) 8.09 (d, J = 8.4 Hz, 2H) ppm. ^{13}C NMR (100 MHz, CDCl$_3$): δ 27.9, 49.6, 55.6, 120.5, 126.0, 127.2, 127.5, 128.9, 129.4, 136.4, 147.6, 160.0 ppm. HRMS (ESI-TOF): m/z calcd for [M + H]$^+$, 371.2191; found, 371.2208.

Synthesis of *N,N′*-bis(pyridin-2-ylmethyl)-*N,N′*-bis(quinolin-2-ylmethyl)butane-1,4-diamine (bqpbn, 1)

200 mg (0.54 mmol) of **H$_2$bqbn** and 4 mL water were placed in a 25 mL RB flask. To this solution, 179 mg (1.09 mmol) of 2-picolyl chloride dissolved in 2 mL water was added dropwise, followed by the addition of 4 equiv. NaOH (88 mg in 2 mL water) in order to maintain the pH close to 12. The resulting mixture was stirred for 24 h at 30 °C. The desired product was extracted with chloroform and then isolated as an off-white solid by evaporating the solvent under reduced pressure. Yield: 269 mg (90%). M.P. 128 °C. ^{1}H NMR (400 MHz, CDCl$_3$): δ 1.55 (t, 4H), 2.54 (t, 4H), 3.81 (s, 4H), 3.94 (s, 4H), 7.11 (t, J = 4 Hz, 2H), 7.51–7.69 (m, 8H), 7.79 (d, J = 7.5 Hz, 2H), 8.03 (d, J = 8.5 Hz, 2H), 8.06 (d, J = 8.5 Hz, 2H), 8.48 (d, J = 4 Hz, 2H) ppm. ^{13}C NMR (100 MHz, CDCl$_3$): δ 24.8, 54.4, 60.5, 61.2, 120.9, 121.9, 122.9, 126.1, 127.3, 127.5, 128.9, 129.3, 136.3, 136.4, 147.4, 148.9, 158.8, 160.0 ppm. HRMS (ESI-TOF): m/z calcd for [M + H]$^+$, 553.3035; found, 553.3012.

Synthesis of *N,N′*-(1,4-phenylenebis(methylene))bis(1-(quinolin-2-yl)methanamine) (H$_2$bqxn)

In a 25 mL RB flask, *p*-Xylylene diamine (136 mg, 1 mmol in 2 mL methanol) was added dropwise to a solution of 2-quinoline carboxaldehyde (314 mg, 2 mmol) prepared in 6 mL of CH$_3$OH, and stirred at 30 °C for 2 h. To this above solution, an excess of NaBH$_4$ (3 equiv., 114 mg) was added step wise at 0 °C, and stirred for 24 h at 30 °C. Upon evaporation of solvent upon reduced pressure, the obtained residue was washed with water and extracted into a chloroform layer. To the organic layer anhydrous Na$_2$SO$_4$ was added, filtered and the desired product was obtained as a yellow solid by evaporating the solvent under reduced pressure. Yield: 368 mg (88%). M.P. 96 °C. ^{1}H NMR (400 MHz, CDCl$_3$): δ 3.94 (s, 4H), 4.15 (s, 4H), 4.24 (s, 4H), 7.40 (s, 4H), 7.49 (d, J = 8.4 Hz, 2H), 7.53–7.72 (m, 4H), 7.83 (d, J = 8.2 Hz, 2H), 8.07 (d, J = 8.4 Hz, 2H), 8.13 (d, J = 8.4 Hz, 2H) ppm. ^{13}C NMR (100 MHz, CDCl$_3$): δ 53.4, 55.1, 120.6, 126.0, 127.3, 127.6, 128.4, 129.0, 129.4, 136.4, 138.9, 147.7, 160.2 ppm. HRMS (ESI-TOF): m/z calcd for [M + H]$^+$, 419.2191; found, 419.2220.

Synthesis of *N,N′*-(1,4-phenylenebis(methylene))bis(1-(pyridin-2-yl)-*N*-(quinolin-2-ylmethyl)methanamine) (bqbpxn, 2)

314 mg (0.75 mmol) of **H$_2$bqxn** was added along with 6 mL water to a 25 mL RB flask. To this, 246.3 mg (1.5 mmol) of 2-picolyl chloride dissolved in 2 mL water was added dropwise, followed by the addition of 4 equiv. NaOH (164 mg in 2 mL water) in order to maintain the pH close to 12. The resulting mixture was stirred for 24 h at 30 °C. The desired product was extracted into a chloroform layer and then isolated as a tan yellow solid by evaporating the solvent under reduced pressure. Yield: 415 mg (92%). M.P. 110–112 °C. ^{1}H NMR (400 MHz, CDCl$_3$): δ 3.74 (s, 4H), 3.88 (s, 4H), 4.00 (s, 4H), 7.15 (t, J = 6.0 Hz, 2H), 7.40 (s, 4H), 7.51 (t, J = 8.0 Hz, 2H), 7.58 (d, 2H), 7.66-7.77 (m, 8H), 8.07 (d, J = 8.0 Hz, 2H), 8.15 (d, J = 8.6 Hz, 2H), 8.52 (d, J = 4.3 Hz, 2H) ppm. ^{13}C NMR (100 MHz, CDCl$_3$): δ 58.4, 60.1, 60.7, 120.9, 122.0, 122.9, 126.1, 127.3, 127.5, 128.9 (2C), 129.4 (2C), 136.4, 137.6, 147.4, 148.9, 159.6, 160.4 ppm. HRMS (ESI-TOF): m/z calcd for [M + H]$^+$, 601.3035; found, 601.3010.

Fluorescence study for nitro-aromatics detection

To a quartz cuvette with a path length of 1 cm, containing 2 mL of Milli-Q water, one milligram of finely ground samples of **1** or **2** was added and stirred at a constant rate to form a uniform suspension. To the above dispersed solution of the samples in water, each nitro explosive was added incrementally from a 1 mM stock solution (stock solutions of these without a phenolic group were prepared in 9.5 mL water and 0.5 mL methanol) and the corresponding photoluminescence spectral responses were monitored by exciting at a wavelength of 340 nm. All experiments were performed three times and consistent results were obtained.

Preparation of a test paper strip

A test paper strip was prepared by coating the fluorescent samples on Whatman filter paper by immersing into an aqueous suspension of the respective samples and dried in air. These strips were used to detect nitro-analytes by dropcasting a small volume of an aqueous solution of each of the nitro-analytes (10 μL, 1 mM in water) onto the dried filter paper strips coated with the samples.

Fluorescence study for metal-ion sensing

To a solution of 32 μM of **1** and **2** prepared in H$_2$O : DMF (1 : 1) solvent, different concentrations of metal ions such as Zn^{2+}, Mn^{2+}, Fe^{2+}, Co^{2+}, Ni^{2+}, Cu^{2+} and Cd^{2+} were added (0 to 64 μM to **1** and 0 to 96 μM to **2**) and the corresponding emission responses were monitored at λ_{exc} = 340 nm.

Results and discussion

Synthesis and characterization

The two sensors **1** and **2** were synthesized by utilizing a combination of Schiff base chemistry and nucleophilic substitution in a two-step procedure in good yields of 90% and 92%,
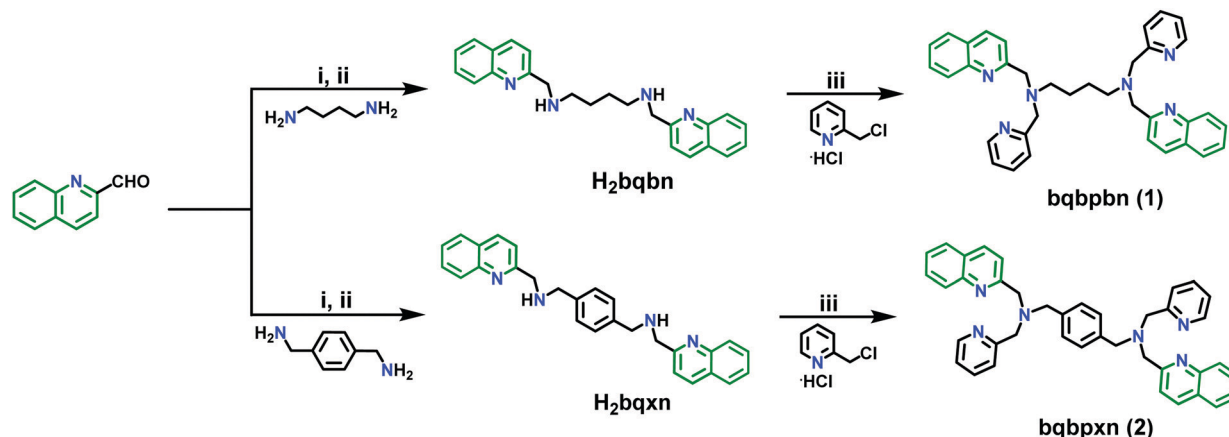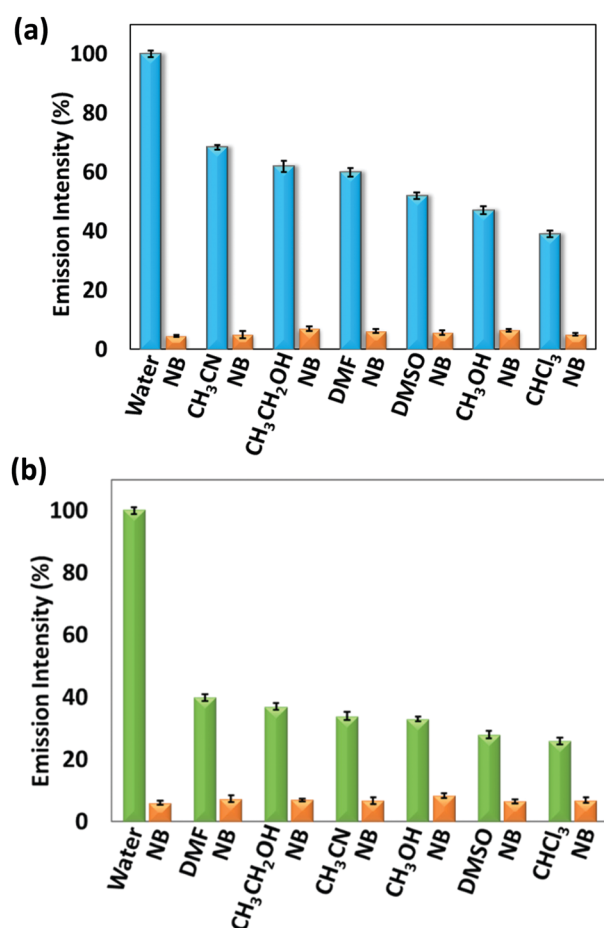
Scheme 2   Synthesis of **1** and **2**: (i) CH$_3$OH, stir, 30 °C, 6 h; (ii) NaBH$_4$ (3 equiv.)/0 °C, stir, 30 °C, 24 h; (iii) H$_2$O, NaOH (4 equiv.), pH = 12, stir, 30 °C, 24 h.

respectively (Scheme 2). The former step involves the reaction of 2-quinoline carboxaldehyde with 1,4-diaminobutane and *p*-xylylenediamine in **1** and **2**, respectively, in a 2 : 1 ratio with a subsequent reduction of the respective imine using sodium borohydride to obtain the reduced Schiff base intermediate H$_2$bqbn and H$_2$bqxn, respectively. The latter step included the nucleophilic substitution reaction under strongly basic conditions to introduce a methylpyridyl moiety at each methyl nitrogen atom of the spacer. These two sensors were thoroughly characterized by melting point (M.P.), high resolution mass spectrometry (HRMS), NMR (^{1}H and ^{13}C), Fourier transform infra-red (FT-IR) and UV-vis spectroscopy (Fig. S1–S15, ESI†). In the ^{1}H spectra of **1** and **2**, the CH$_2$ groups attached to 2-pyridyl and quinoline appear as singlets at 3.81/3.88 ppm and 3.94/4.00 ppm, respectively (Fig. S4 and S10, ESI†). In the FT-IR spectra of **1** and **2**, no residual peaks for the functional groups CHO and NH were observed indicating purity of the products (Fig. S13 and S14, ESI†). Furthermore, the HRMS data exhibited the expected molecular ion peaks. It is noteworthy to mention that the synthesis of **1** under ambient conditions in H$_2$O is much greener compared to that (reflux conditions in dry CH$_3$CN and under a dinitrogen atmosphere) used for a similar compound **L^2** (*N*,*N*′-bis(2-quinolinylmethyl)-*N*,*N*′-bis(2-pyridylmethyl) propylendiamine), which was reported for metal ion sensing.[64f] On the other hand, few compounds containing only quinoline moieties with an aliphatic cyclohexyl or methylene spacer between two secondary amino nitrogens (reduced Schiff bases) have been reported as fluorescent pH indicators.[64g] Thus, the design of **2** is different from these compounds, as it also contains a Lewis basic pyridyl moiety acting as a recognition site for NACs *via* H-bonding and an aromatic electron-rich xylylene spacer between two alkyl nitrogens providing π–π interaction with NACs.

Effect of solvents on emission spectra

To study the effect of solvents on the emission intensity of **1** and **2**, their solid-state fluorescence spectra were recorded by exciting at 340 nm (Fig. S16, ESI†). For **1**, an emission was observed at 428 nm while for **2**, two broad peaks appeared at 449 nm and 553 nm with significantly low intensity for self-quenching compared to **1**. This depicts that the emission in **2** is due to the formation of excimer resulting in self-aggregation for which more broad and red-shifted peaks are observed. This can be attributed to the presence of an aromatic xylylene moiety, which is capable of forming π–π interactions resulting in self-aggregation based quenching in

Fig. 1   Change in emission intensity % after addition of nitrobenzene to (a) **1** and (b) **2** in the presence of different solvents.

the solid state. By utilizing the solid-state fluorescent property of **1** and **2**, their sensing ability towards different solvents, such as water (H_2O), acetonitrile (CH_3CN), ethanol (CH_3CH_2OH), methanol (CH_3OH), chloroform ($CHCl_3$), dimethylformamide (DMF) and dimethylsulfoxide (DMSO) were analysed (Fig. S17, ESI†). These two sensors were soluble in CH_3CN, CH_3CH_2OH, CH_3OH, $CHCl_3$, DMF and DMSO but insoluble in H_2O. In both cases, maximum intensity was observed in H_2O that can be attributed to aggregation-induced emission. Compared to H_2O, the emission response in other solvents were observed at lower intensity with red shifts that may be related to the solubility difference of **1** and **2** in different solvents, leading to some extent of quenching. Their quantum yields measured by dispersing in water and in CH_3CN solution are 0.044 (**1**) and 0.035 (**2**), and 0.0092 (**1**) and 0.0084 (**2**), respectively. Furthermore, for demonstrating the aggregation-induced emission in the presence of H_2O, different volume fractions of water were added to a fixed concentration of **1** and **2** in THF (32 μM) that resulted in a proportional increase in intensity with the water content

(Fig. S18, ESI†). Moreover, for the effect of a nitro group containing solvent in the presence of different solvents, namely nitrobenzene (NB), 1 mL was added to the dispersed solution of **1** and **2** in water (1 mL). It was observed that the emission intensity percentage decreased to a larger extent upon addition of NB in both **1** and **2** (Fig. 1). This can be anticipated due to the electron withdrawing nature of NB which interacts with the electron-rich organic sensors.

Sensing of NACs

Motivated by the aforementioned results for solvents, particularly nitrobenzene, fluorescence titration studies were carried out for different NACs such as, 2,4,6-trinitrophenol (TNP), 2,4-dinitrophenol (2,4-DNP), 4-nitrophenol (4-NP), 2,4,6-trinitrotoluene (TNT), 2,6-dinitrotoluene (2,6-DNT), 2,4-dinitrotoluene (2,4-DNT), 1,3-dinitrobenzene (1,3-DNB) and NB, owing to their electron-deficient nature. For these experiments, water was selected as the solvent medium and 1 mg of each of the sensors were dispersed in 2 mL water (Milli-Q) in order to facilitate close proximity between the sensors and NACs. The excitation spectra of **1** and **2** dispersed in water were recorded and compared with their respective solid-state diffuse-reflectance spectra (Fig. S19,
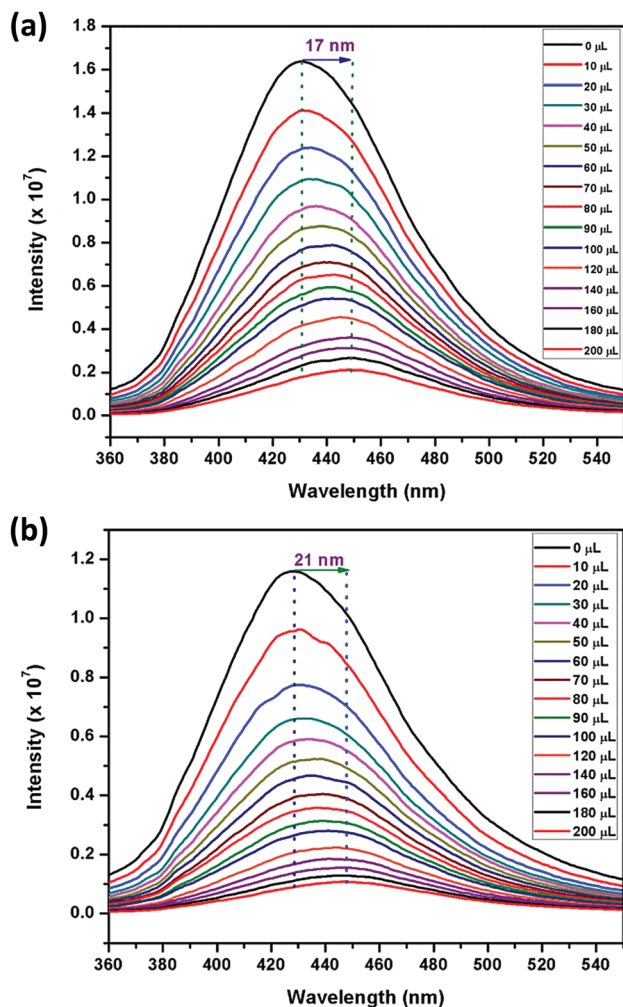
Fig. 2 Effect on the emission spectra of (a) **1** and (b) **2** dispersed in Milli-Q water (1 mg, 2 mL) upon incremental addition of TNP (1 mM) (λ_{exc} = 340 nm).
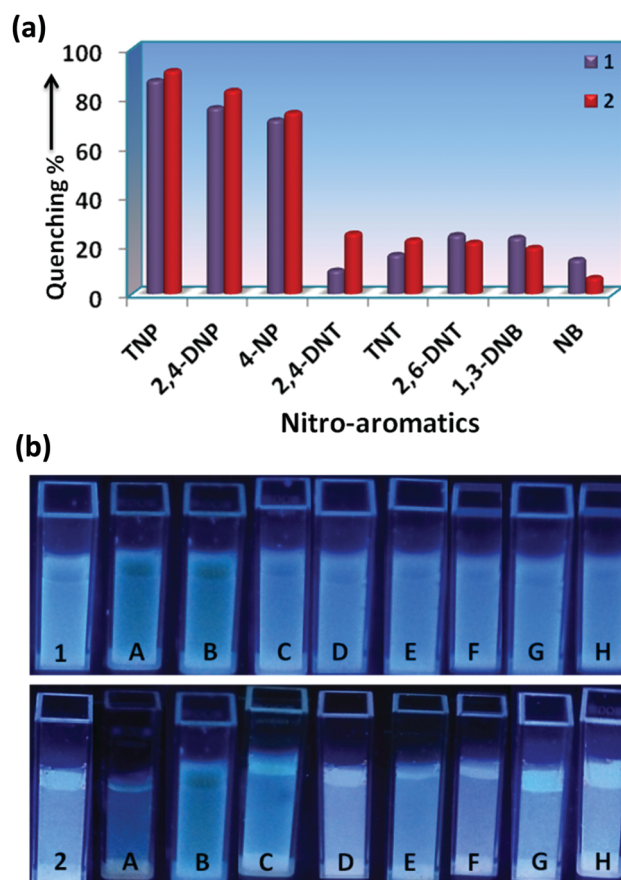
Fig. 3 (a) Fluorescence quenching (%) of **1** and **2** dispersed in water (1 mg, 2 mL) by different NACs (200 μL, 1 mM). (b) Cuvette photographs of **1** and **2** before and after the addition of 200 μL of different analytes upon UV-light illumination at λ = 365 nm, where, A: TNP; B: 2,4-DNP; C: 4-NP; D: 2,4-DNT; E: TNT; F: 2,6-DNT; G: 1,3-DNB; H: NB.

ESI†). The excitation spectra have very similar shape but are red-shifted due to the use of polar water as the solvent. To these suspensions, NACs were gradually added from 1 mM stock solutions (0–200 μL) and the emission intensities were monitored at 429 nm and 427 nm, respectively, in **1** and **2** (Fig. 2 and Fig. S20–S33, ESI†). Upon incremental addition of TNP, a large bathochromic shift of 17 nm and 21 nm was observed followed by a decrease in intensity in the emission spectra of **1** and **2**, respectively. This red shift in wavelength can be attributed to either energy transfer or electrostatic interaction occurring between the electron-rich sensors and the electron-deficient TNP.[71]

The incremental addition of different NACs (1 mM) up to 200 μL, has resulted in different extents of fluorescence quenching (λ_{exc} = 340 nm). The quenching efficiency percentage was evaluated by using the equation: $(I_0 - I)/I_0 \times 100\%$, where I_0 and I are the emission intensities of the sensors before and after addition of the nitro-aromatics, respectively (Fig. 3a). It was observed that for 200 μL (1 mM) addition of TNP, the quenching % was 87% and 91%, for **1** and **2**, respectively. The distinct change in color particularly in the case of TNP was also observed in **1** and **2** in the presence of different NACs after irradiation with UV-light (λ = 365 nm) (Fig. 3b). This clearly indicates that the semi-rigid spacer xylylene is playing a role in increasing the interaction with the TNP.

Mechanism of action for TNP detection

To acquire better understanding about the principle behind the selective detection of TNP, the possible quenching mechanisms were investigated. First, the Stern–Volmer quenching constants were evaluated by using the Stern–Volmer (SV) equation: $I_0/I = 1 + K_{SV}[A]$, where, I_0 is the initial emission intensity without the nitro-analyte, I is the emission intensity with the addition of the nitro-analyte of molar concentration [A] and K_{SV} is the quenching constant (Fig. 4). An upward bend curve was observed at higher concentration with linearity at a lower concentration in the SV plot for TNP and 2,4-DNP in **1** and **2** (Fig. S34–S37, ESI†). This non-linearity can be allocated to self-absorption or an energy transfer process between the sensor and analyte.[1,32,62] In comparison, the SV plots for other analytes are almost a linear curve, thereby suggesting that either static or dynamic quenching is involved.[72] For TNP, the K_{SV} values were found to be $(3.55 \pm 0.09) \times 10^4$ and $(4.97 \pm 0.08) \times 10^4$ M⁻¹, respectively in **1** and **2** (Fig. S38 and S39, ESI†). The detection limits of TNP were also evaluated to be 1.2 ppm and 0.3 ppm in **1** and **2**, respectively (Fig. S40 and S41 and Tables S1–S2, ESI†).

On comparing the quenching in **1** and **2** (Table S3, ESI†), it is found that they correlate well with the order of their acidity: TNP > 2,4-DNP > 4-NP. These values are found in the order of 3.55×10^4 M⁻¹ (TNP) > 3.14×10^4 M⁻¹ (2,4-DNP) > 1.90×10^4 M⁻¹ (4-NP) in **1** and in the order of 4.97×10^4 M⁻¹ (TNP) ≫ 2.49×10^4 M⁻¹ (2,4-DNP) > 2.02×10^4 M⁻¹ (4-NP) in **2**. This can be ascribed to the availability of nitrogen atoms from Lewis basic pyridyl and quinoline sites which are capable of forming hydrogen bonding interactions with the acidic hydroxyl groups of nitro-phenol derivatives, which is not
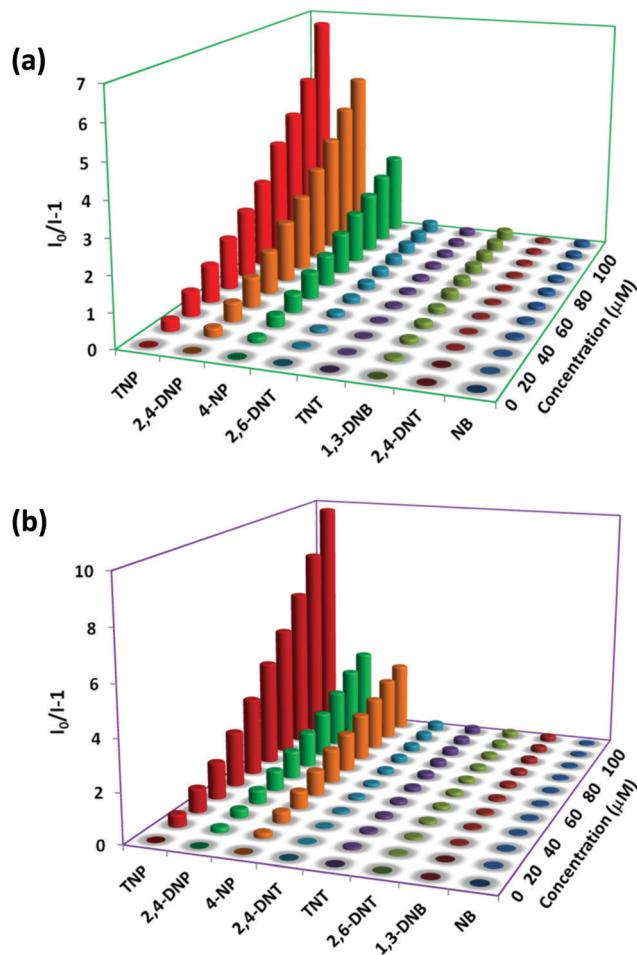

Fig. 4 Stern–Volmer plots for different NACs in **1** (a) and **2** (b) dispersed in water (1 mg, 2 mL).

possible in other NACs.[24] It is also apparent from the K_{SV} values for TNP that the extent of interaction in **2** is more compared to **1**. The detection limit for TNP (0.3 ppm) in **2** is found to be slightly better than that of the reported quinoline-based probe, 2,5-dimethylbis(quinolin-2-ylmethylene) benzene-1,4-diamine (DQB) (0.34 ppm), possibly due to the extra Lewis basic pyridyl groups in **2** (Table S4, ESI†).[70b] Also, the detection limit of **2** is higher and comparable with other probes performed in water such as organic probes: H₂ATAIA (120 ppb),[32] H₂AMTAIA (0.8 ppm),[32] H₂DMTAIA (1.2 ppm)[32] and naphthalene-based compound 1 (3.48 ppm)[24] and MOF based probes: [Zn(NDC)H₂O]ₙ (0.23 ppm) and [Cd(NDC)(H₂O)]ₙ (0.92 ppm), {[Zn₈(ad)₄(BPDC)₆O·2Me₂NH₂]·G}ₙ (0.2 ppm) and UiO-68-NH₂ (0.4 ppm), etc.[45–49] The K_{SV} values of **1** and **2** are higher than other reported organic probes such as probes tagged with naphthalene (3.43×10^3 M⁻¹ and 2.69×10^4 M⁻¹),[24,25] benzimidazole (1.58×10^4 M⁻¹),[27] anthracene (1.77×10^4 M⁻¹)[16] and fluorescein (2.10×10^4 M⁻¹)[31] and comparable with that of other anthracene (8.08×10^4 M⁻¹ and 7×10^4 M⁻¹),[25,32] fluorene (3.90×10^4 M⁻¹)[16] and MOF probes such as [Tb(BTC)]ₙ (3.9×10^4 M⁻¹),[49c] {Zr₆O₄(OH)₄(L)₆}ₙ (2.9×10^4 M⁻¹),[45] [Cd(NDC)₀.₅(PCA)]ₙ (3.9×10^4 M⁻¹)[40] and TB-Zn-CP (4.37×10^4 M⁻¹)[49d] based sensors (Table S4, ESI†). On comparing the

detection limits with the two sensors recently reported by our group,[62] it was observed that the sensing ability is improved by the variation of the spacer and increasing Lewis basic nitrogen sites. In addition, the K_{SV} value of **1** is higher than its naphthalene analogue (3.26×10^4 M^{-1}).[62] To further introspect into the sensing mechanism, the extent of spectral overlap between the absorbance spectra of the NACs (0.03 mM) and the emission spectra of **1** and **2** was analysed. The larger extent of overlap signifies greater quenching efficiencies of NACs, and in both cases more overlap was observed in the case of TNP followed by 2,4-DNP and 4-NP with no overlap for other nitro-analytes (Fig. 5). This confirms that resonance energy transfer (a long-range phenomenon) is occurring from the electron-rich sensors to the electron deficient acidic nitro-phenol derivatives with the subsequent drastic increase in the quenching efficiency. Furthermore, spectral overlap integral values were calculated in **1** and **2** with TNP,[72] and were found to be 2.35×10^{14} and 2.48×10^{14} M^{-1} cm^{-1} nm^4 for **1** and **2**, respectively. This demonstrates that there is slightly more resonance energy transfer in **2** compared to **1**, as predicted due to the presence of xylylene spacer in **2**. Furthermore, due to spectral overlap, the IFE can also exist to some extent and contribute to the quenching process. There are reports in the past where the correction factor for IFE is described for solution systems.[73] In recent times, this effect has been utilized as one of the sensing tools in which due to absorbance changes of the absorber translate exponentially into fluorescence intensity changes that results in a better sensitivity of this method compared to other methods.[74] However, these effects do not strongly dictate the greater Ksv value and better detection limit in **2**.

This prompted us to calculate the HOMO–LUMO energies of **1**, **2** and NACs using density functional theory (DFT) with the B3LYP/6-31G+(d,p) basis set and the Gaussian 09 package program.[75] The energy-minimized structures for **1** and **2** were determined using this program as shown in Fig. S42 (ESI†). The distance between the alkyl nitrogen atoms connecting the methylene groups in **1** and xylylene group in **2** is 6.338 and

7.609 Å, respectively, which reflects the effect of the semi-rigid xylylene spacer preventing the molecule shrinking.

In principle, the analyte possessing lower energy of the LUMO has a greater probability of getting an electron transferred from the excited state of the fluorophore and thereby leading to fluorescence quenching (Fig. 6a).[4] The HOMO–LUMO energy gaps shown in Fig. S43 and Table S5 (ESI†) depicts that the LUMO of TNP is lower than that of the other nitro-analytes, making it a target analyte for better sensing.

Fig. 6 (a) Schematic illustration of the quenching mechanism *via* photo-induced electron transfer. (b) Calculated energy diagram with the HOMO–LUMO energies of **1**, **2** and TNP. (c) Possible mechanism of TNP sensing in (i) **1** and (ii) **2**.
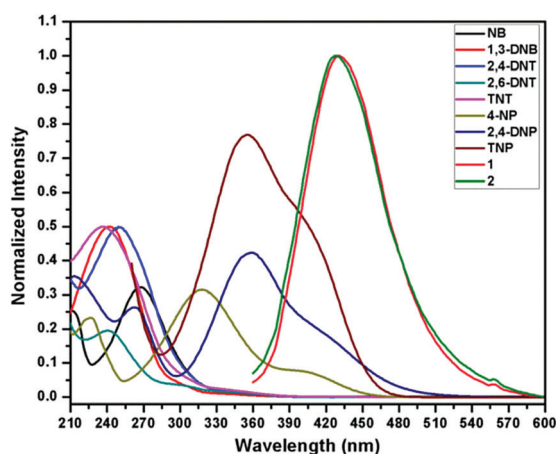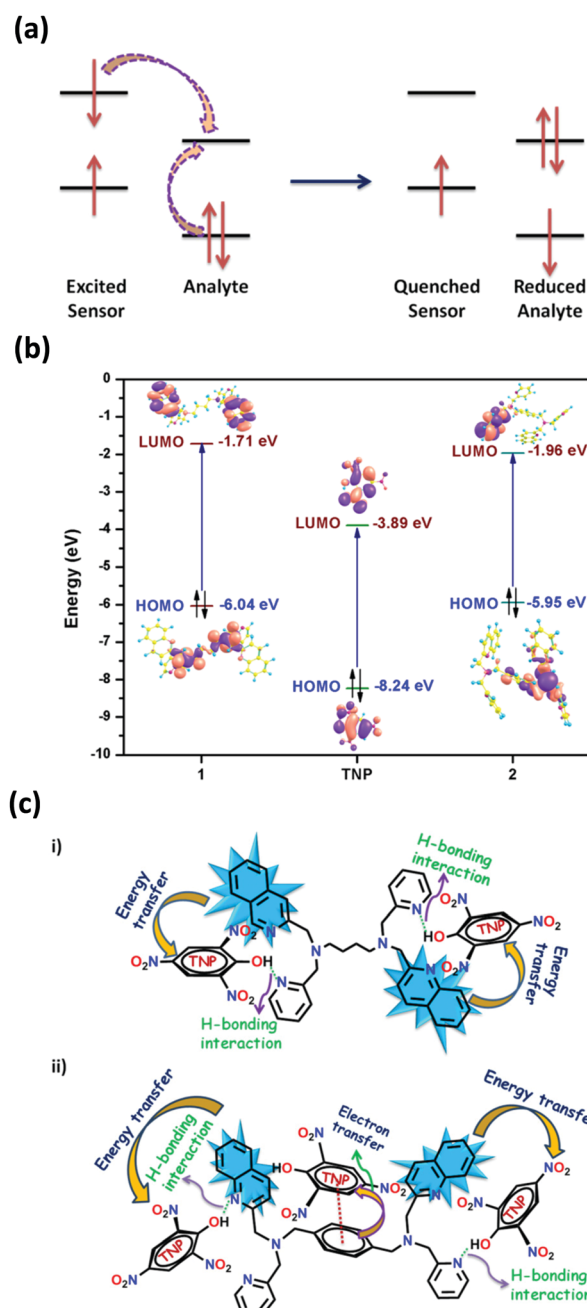

Fig. 5 Spectral overlap of absorption spectra of different NACs and emission spectra of **1** and **2** dispersed in water.

Paper

Also, it is noteworthy to observe that the LUMO of **2** is lower in energy compared to **1** (Fig. 6b). This vividly shows that upon excitation of an electron from the HOMO to the LUMO of **2** it can result in electron transfer more easily to the LUMO of TNP. Therefore, it can be determined that the electron transfer has a more profound effect compared to energy transfer during the sensing of TNP due to the presence of an electron rich xylylene spacer in **2** compared to an aliphatic flexible tetra-methylene spacer in **1** (Fig. 6c). Moreover, to validate the proposed mechanism, calculations were performed to understand the interaction between **1** or **2** and TNP using the DMol3 module of the Material Studio program.[76] Different optimized structures are shown in Fig. 7. It is observed that both pyridyl and quinoline nitrogens are capable of forming H-bonding interactions with the hydroxyl group of TNP in **1** and **2** (Fig. 7a and b, respectively). The N···H–O distances were found to be in the range of 2.2 to 2.95 Å and the H-bonding is more predominant with pyridine N compared to quinoline N. In addition, the quinoline and the xylylene moieties in **2** also efficiently participate in the π–π interaction with the phenyl ring of TNP (3.462 and 3.507 Å) as shown in Fig. 7c. These data correlate well with the possible mechanism as stated above, where the strong π–π interaction with quinoline/xylylene and TNP adduct leads to intermolecular charge transfer, which results in further

red-shifting of the emission maximum for **2**.[70b] Furthermore, any other contribution, such as IFE, to the quenching process can be very minor for the use of the very low concentration of the sensors (1 mg solid dispersed in 2 mL water) used in this study; no quantification of this minor contribution was made as it is also not practical for solid probes dispersed in a solvent, and it is not easy to find a nonaromatic species for a control experiment that has the same absorption at the excitation wavelength as TNP but will not interact with the sensors containing aromatic moieties.[73]

Time-resolved lifetime measurements. To further understand the mechanism of quenching in **1** and **2**, their lifetime decay profiles were recorded before and after the addition of TNP (Fig. 8). In both cases, the average lifetime was calculated using the formula:

$$\langle\tau\rangle = (\alpha_1\tau_1{}^2 + \alpha_1\tau_2{}^2 + \alpha_3\tau_3{}^2)/(\alpha_1\tau_1 + \alpha_2\tau_2 + \alpha_3\tau_3)$$

where, $\langle\tau\rangle$ is the average lifetime and α is the pre-exponential factor with subscripts 1, 2 and 3 representing various species. Based on these data, the average lifetimes for **1** were 5.41 ns (before the TNP addition), 5.28 ns (after 20 μL TNP addition), 4.19 ns (after 40 μL TNP addition) and 3.02 ns (after 200 μL TNP addition), whereas for **2** the values were 5.05 ns (before the TNP
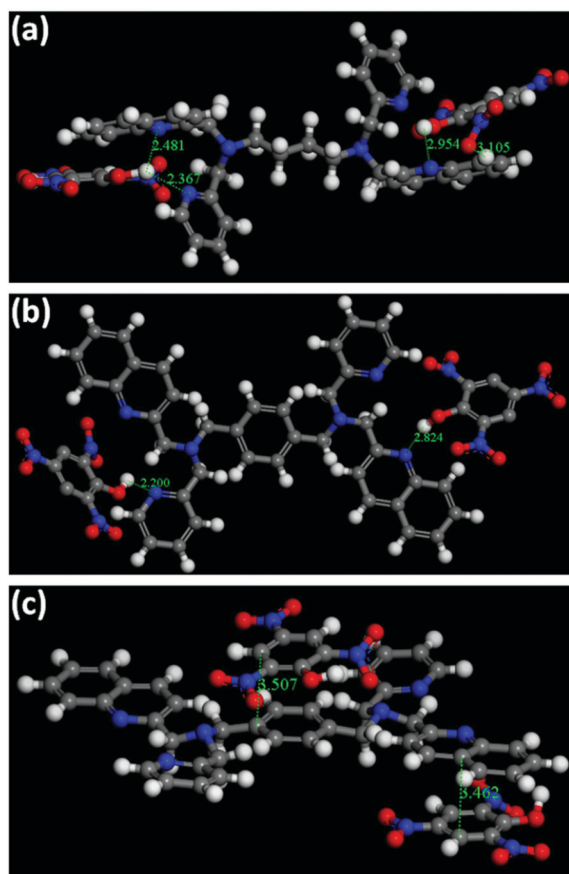

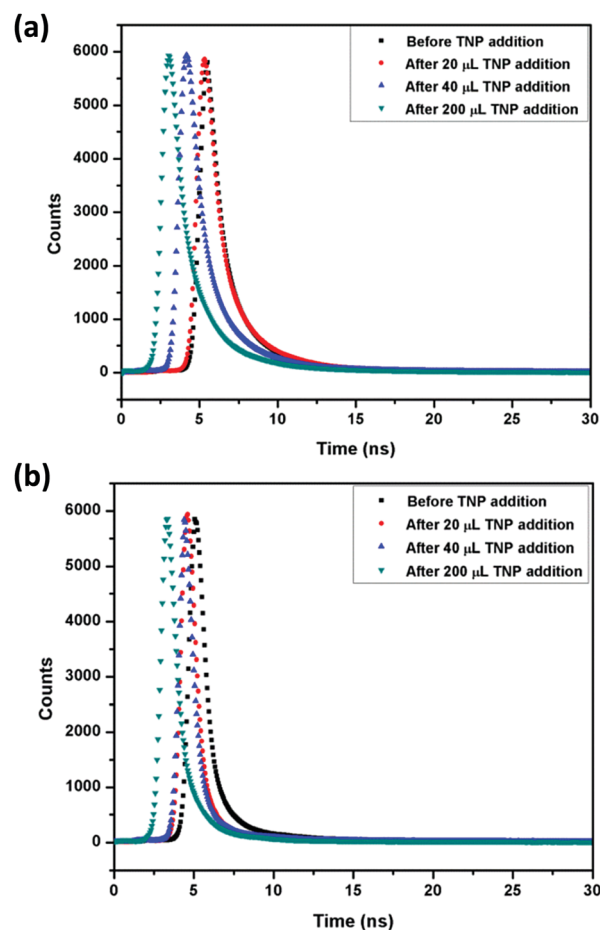Fig. 7 Different interactions observed in **1** (a) and **2** (b and c) calculated by the DMol3 module.

Fig. 8 Lifetime decay profiles of **1** (a) and **2** (b) before and after the addition of TNP.

addition), 4.60 ns (after 20 μL TNP addition), 4.37 ns (after 40 μL TNP addition) and 3.29 ns (after 200 μL TNP addition) (Fig. 8 and Table S6, ESI†). The quenching rate constant (K_q) values were also found to be 6.56×10^{12} and 9.84×10^{12} M^{-1} s^{-1}, respectively, for **1** and **2** using the following equation: $K_q = K_{SV}/\langle\tau\rangle$, where K_{SV} is the quenching constant and $\langle\tau\rangle$ is the average lifetime of the sensor. $\langle\tau\rangle$ shows that in the case of **1**, initially there is very little change in lifetime after addition of 20 μL of TNP followed by a substantial decrease in lifetime with 40 μL and 200 μL addition of TNP, indicating static quenching[72] at lower concentrations and dynamic quenching at higher concentrations. On the other hand, in **2** there is a considerable decrease in lifetime from lower to higher concentrations with the addition of TNP demonstrating dominance of dynamic quenching throughout the process.[72] This also corroborates well with the aforementioned results and explains that there is more electron transfer in **2** compared to **1**, further justifying the role of the semi-rigid xylylene spacer.

Selectivity, stability and recyclability test. To investigate the competitive behavior of TNP in the presence of other nitro-analyte congeners, the selectivity test was performed for **1** and **2**. In a typical fluorescence experiment, the emission intensity of sensors (1 mg dispersed in 2 mL water) was recorded before and after the addition of 100 μL of a particular NAC followed by the addition of 100 μL of TNP (1 mM, H$_2$O). A moderate to slight change in emission intensity of **1** and **2** was observed for other NACs, while a significant and noteworthy decrease in intensity took place after the addition of TNP. These results reassured TNP selectivity over other non-phenolic NACs even at higher concentrations (Fig. 9).

The hydrolytic and chemical stability of **1** and **2** in water and acidic TNP, respectively, were confirmed by PXRD and FESEM. For these studies, about 15 mg of each sample was immersed in 2 mL of water or aqueous TNP solution for 3 days, filtered and washed rigorously with water. Comparing the PXRD patterns of these treated samples with that of the pristine samples confirmed the structural integrity in both cases even after such exposure as shown in Fig. S44 (ESI†). In addition, field-emission scanning electron microscopy (FE-SEM) was also utilized, indicating no morphological changes before and after soaking in an aqueous solution of TNP (1 mM) (Fig. S45, ESI†). Furthermore, the recyclability test was performed by recovering **1** and **2** after every fluorescence experiment by centrifugation and washing with water several times. These were then again used for quenching experiments of TNP for up to five cycles that showed the retention of their fluorescence intensity and quenching ability without much loss of sensitivity (Fig. S46, ESI†).

On-site detection of TNP for practical applications. The detection of TNP in the solid state was performed for in-field applications. For this purpose, test paper strips were prepared by encrusting the sensors dispersed in water on Whatman filter paper. These test strips also showed strong emission in the blue region upon excitation at 365 nm under UV light. After drop casting a small amount of each NAC as a spot on these test strips, a recognizable change was observed for TNP only as a dark color and adequate darkening took place in the presence
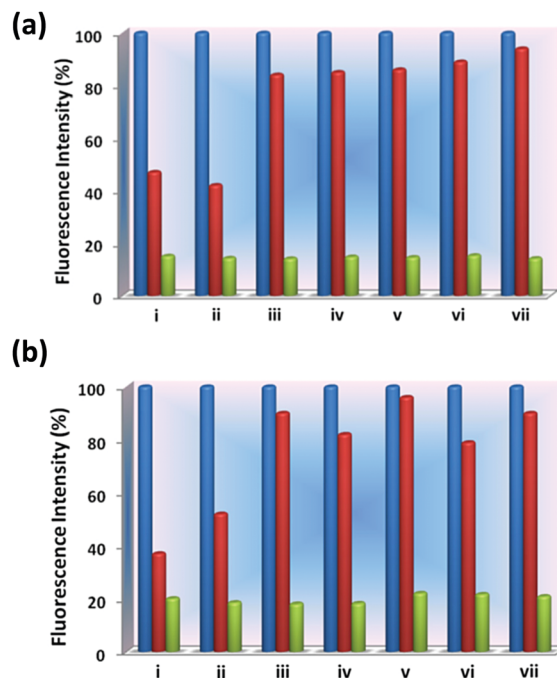

Fig. 9 Bar diagrams of the fluorescence intensity (%) of **1** (a) and **2** (b) in the absence and presence of NACs separately followed by the addition of the same amount of TNP. Blue bars represent the suspension of compounds in water, red bars represent the addition of various nitroanalytes to the suspension of the pristine (compound + nitro-analytes), and green bars represent the subsequent addition of TNP (100 μL, 1 mM) to the abovementioned suspensions (compound + nitro-analytes + TNP); from left to right (i) 2,4-DNP, (ii) 4-NP, (iii) TNT, (iv) 2,6-DNT, (v) 2,4-DNT, (vi) 1,3-DNB, and (vii) NB.

of 2,4-DNP and 4-NP, whereas other NACs showed an insignificant change (Fig. 10a). This showed that TNP can be discriminated from other NACs for on-site detection. Inspired from these results, different concentrations of TNP were added to the test strips coated with **1** and **2** (10 μL each, 10^{-8} to 10^{-3} M), that led to the incremental darkening of spots with the increase in concentration of TNP upon UV illumination at 365 nm (Fig. 10b). Also, it is noteworthy to observe that in **1** appreciable darkening occurs at a concentration of 10^{-4} M whereas in **2** initial darkening takes place even at a concentration of 10^{-6} M, corroborating with the better
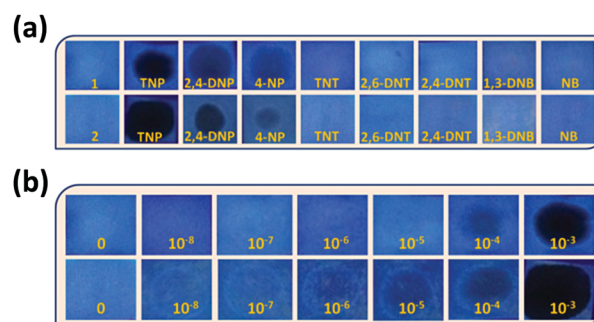

Fig. 10 (a) Paper strips encrusted with **1** (top) and **2** (bottom) and their respective visualisation in the presence of different NACs under UV light (λ = 365 nm). (b) Photographs of paper strips coated with **1** (top) and **2** (bottom) with increasing concentration of TNP (10^{-8} to 10^{-3} M).
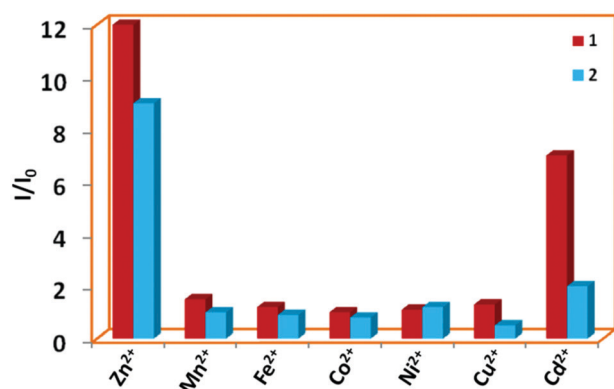
Fig. 11 Bar plot for relative emission intensities of **1** and **2** in the presence of one and two equivalents of metal ions in DMF : H$_2$O (1 : 1), respectively.

detection limit in **2** compared to **1**. This study demonstrated that **1** and **2** have high sensitivity towards TNP for practical applications *via* visual detection with the naked eye. These results are highly comparable and better than previously reported TNP sensor-based systems.[46,47d,50,77]

Sensing of metal ions

Several quinoline based probes are reported in the literature for metal ion sensing.[63–69] Based on this information and the presence of six N-donor sites in **1** and **2** for chelation with the metal centers, the effect of flexible *vs.* semi-rigid spacers is further established through sensing of metal ions by fluorescence spectroscopy (excited at 340 nm and monitored at 410 and 419 nm, respectively). Compared to other metal ions, **1** and **2** exhibited fluorescence enhancements toward Zn^{2+} followed by Cd^{2+} due to chelation-enhanced fluorescence of closed-shell d^{10} metals which diminishes the PET process (Fig. 11).[64e] The binding affinity Zn^{2+} with N centres of pyridine and quinoline is much more favourable compared to Cd^{2+} and indicates a much higher selectivity of **1** and **2** for Zn^{2+} over the other metal ions.[64b] Due to steric hindrance for the larger ionic radii of Cd^{2+}, it may lead to quenching in the presence of enhanced emission of Zn^{2+} *via* electron or energy transfer. This has been observed in other similar reported quinoline-based probes.[64a,b,h]

Focusing on the Zn^{2+} ion, the sensitivity of **1** and **2** (32 μM, 1 : 1 H$_2$O:DMF) was established by titration experiments (Fig. 12a and b). Upon the addition of 0.0025 equivalent of Zn^{2+} (5 ppb) to **1**, the intensity was enhanced by 5.2%, whereas 0.005 equivalent (10 ppb) of Zn^{2+} for **2** enhanced the intensity by 3.5%. These detection limits for **1** and **2** are among the best reported for other similar sensors and are significantly lower than environmental allowance.[63] The gradual increase in fluorescence intensity was observed for up to one equivalent
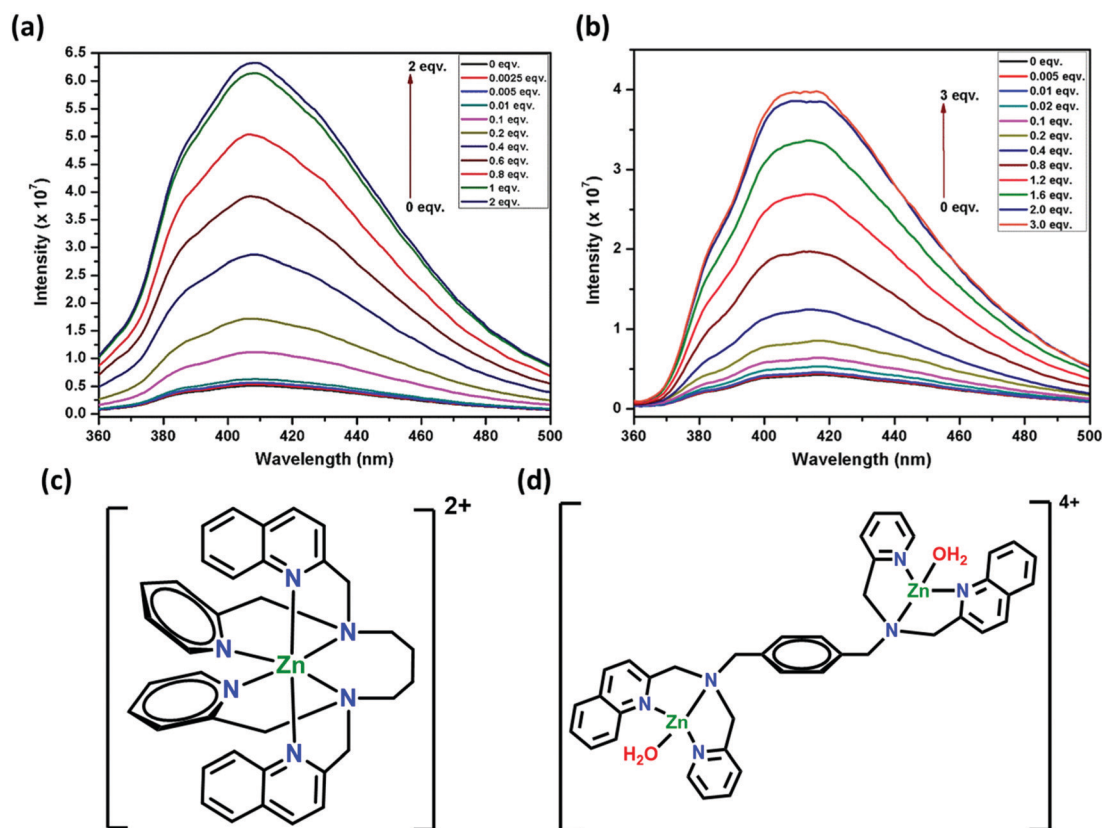

Fig. 12 Emission spectra of (a) **1** and (b) **2** (32 μM) in DMF : H$_2$O (1 : 1) with an increase in concentration of Zn^{2+} ranging from 0 to 64 μM and 0 to 96 μM, respectively (λ_{exc} = 340 nm). Schematic representation of 1 : 1 and 1 : 2 complex formation in the presence of one and two equivalents of Zn^{2+} ion for **1** (c) and **2** (d), respectively.

of Zn^{2+} ions for **1** and two equivalents of Zn^{2+} ions for **2**. Further addition of Zn^{2+} to **1** or **2** (up to two or three equivalents, respectively) did not change the intensity appreciably. This can be corroborated with the formation of a 1 : 1 adduct for **1** (Fig. 12c), which is also proposed[64f] for a similar fluorescent sensor L^2. In the case of **2**, a 1 : 2 adduct is formed (Fig. 12d). This can be attributed to the presence of the semi-rigid xylylene moiety that does not allow the six N-donor sites to span around the Zn center, which is possible in **1** due to the presence of a flexible tetra-methylene chain. Also, the turn-on efficiency of **1** was better compared to **2** due to (i) the faster zinc complexation rate of **1** for the presence of flexible tetra-methylene moiety and (ii) the aggregation of xylylene moiety after complex formation, which is absent in **1**.

Conclusions

In summary, two new sensors based on quinoline and pyridyl groups with a variation in spacer from tetra-methylene in **1** to xylylene in **2** have been successfully developed and synthesized under ambient reaction conditions. Both have high selectivity towards nitro-phenolic compounds, particularly high sensitivity towards TNP with the detection limits of 1.2 ppm and 0.3 ppm, respectively in **1** and **2**. By the utilization of various techniques it is evident that PET, energy transfer, IFE and electrostatic interactions play important roles in the sensing of TNP. However, PET has a superior effect in **2** due to the presence of a semi-rigid xylylene spacer which is not possible in **1** because of the presence of a flexible tetra-methylene chain. For this effect, a better detection limit and quenching constant is obtained for TNP in **2**. Both **1** and **2** exhibited competitive selectivity in the presence of other NACs. Their stability in water and after immersing in TNP was confirmed by PXRD and FESEM, respectively. For on-site detection of TNP, test paper strips were prepared encrusted with **1** and **2**, revealing that these are capable for practical application *via* visual imaging and are promising candidates for pollution control. Also, the metal ion sensing experiments reveal that the emission intensity of **1** and **2** was selectivity enhanced by Zn^{2+} ions compared to other metal ions, resulting into the formation of 1 : 1 and 1 : 2 adducts, respectively. This further confirmed the effect of the flexible tetra-methylene chain in **1** and semi-rigid xylylene moiety in **2**. Further developments for designing potential probes with better efficacies and sensitivity are in progress in our laboratory.

Conflicts of interest

There are no conflicts to declare.

Acknowledgements

References

1 Y. Salinas, R. Martinez-Manez, M. D. Marcos, F. Sancenon, A. M. Costero, M. Parra and S. Gil, *Chem. Soc. Rev.*, 2012, **41**, 1261–1296.

2 D. Banerjee, Z. Hu and J. Li, *Dalton Trans.*, 2014, **43**, 10668–10685.

3 Z. Hu, B. J. Deibert and J. Li, *Chem. Soc. Rev.*, 2014, **43**, 5815–5840.

4 (*a*) S. S. Nagarkar, A. V. Desai and S. K. Ghosh, *CrystEngComm*, 2016, **18**, 2994–3007; (*b*) J.-Q. Liu, Z.-D. Luo, Y. Pan, A. K. Singh, M. Trivedi and A. Kumar, *Coord. Chem. Rev.*, 2020, **406**, 213145.

5 W. P. Lustig, S. Mukherjee, N. D. Rudd, A. V. Desai, J. Li and S. K. Ghosh, *Chem. Soc. Rev.*, 2017, **46**, 3242–3285.

6 M. E. Germain and M. J. Knapp, *Chem. Soc. Rev.*, 2009, **38**, 2543–2555.

7 X. Sun, Y. Wang and Y. Lei, *Chem. Soc. Rev.*, 2015, **44**, 8019–8061.

8 P. Ghosh, J. Das, A. Basak, S. K. Mukhopadhyay and P. Banerjee, *Sens. Actuators, B*, 2017, **251**, 985–992.

9 F.-Y. Yi, D. Chen, M.-K. Wu, L. Han and H.-L. Jiang, *ChemPlusChem*, 2016, **81**, 675–690.

10 S. S. Nagarkar, A. V. Desai and S. K. Ghosh, *CrystEngComm*, 2016, **18**, 2994–3007.

11 J. Pichtel, *Appl. Environ. Soil Sci.*, 2012, **2012**, 1–33.

12 J. Akhavan, *The Chemistry of Explosives*, Royal Society of Chemistry, Cornwall, UK, 2004.

13 A. W. Czarnik, *Nature*, 1998, **394**, 417–418.

14 K. M. Wollin and H. H. Dieter, *Arch. Environ. Contam. Toxicol.*, 2005, **49**, 18–26.

15 K. W. Hofmann, H.-J. Knackmuss and G. Heiss, *Appl. Environ. Microbiol.*, 2004, **70**, 2854–2860.

16 P. G. Del Rosso, M. J. Romagnoli, M. F. Almassio, C. A. Barbero and R. O. Garay, *Sens. Actuators, B*, 2014, **203**, 612–620.

17 S. Hussain, A. H. Malik, M. A. Afroz and P. K. Iyer, *Chem. Commun.*, 2015, **51**, 7207–7210.

18 W. Huang, E. Smarsly, J. Han, M. Bender, K. Seehafer, I. Wacker, R. R. Schröder and U. H. F. Bunz, *ACS Appl. Mater. Interfaces*, 2017, **9**, 3068–3074.

19 H.-T. Feng and Y.-S. Zheng, *Chem. – Eur. J.*, 2014, **20**, 195–201.

20 Y. Z. Fana, Y. Zhanga, N. Li, S. G. Liu, T. Liu, N. B. Li and H. Q. Luo, *Sens. Actuators, B*, 2017, **240**, 949–955.

21 L. Lin, M. Rong, S. Lu, X. Song, Y. Zhong, J. Yan, Y. R. Wang and X. Chen, *Nanoscale*, 2015, 7, 1872–1878.

22 Y. Peng, A.-J. Zhang, M. Dong and Y.-W. Wang, *Chem. Commun.*, 2011, **47**, 4505–4507.

23 P. Ghosh, S. Paul and P. Banerjee, *CrystEngComm*, 2017, **19**, 6703–6710.

24 S. Mukherjee, A. V. Desai, A. I. Inamdar, B. Manna and S. K. Ghosh, *Cryst. Growth Des.*, 2015, **15**, 3493–3497.

25 A. Sil, D. Giri and S. K. Patra, *J. Mater. Chem. C*, 2017, **5**, 11100–11110.

26 V. Lakshmidevi, C. V. Yelamaggad and A. Venkataraman, *ChemistrySelect*, 2018, **3**, 2655–2664.

27 S. Joshi, S. Kumari, E. Chamorro, D. D. Pant and R. Sakhuja, *ChemistrySelect*, 2016, **1**, 1756–1762.

28 K. Maiti, A. K. Mahapatra, A. Gangopadhyay, R. Maji, S. Mondal, S. S. Ali, S. Das, R. Sarkar, P. Datta and D. Mandal, *ACS Omega*, 2017, **2**, 1583–1593.

29 S. C. Deshmukh, S. Rana, S. V. Shinde, B. Dhara, N. Ballav and P. Talukdar, *ACS Omega*, 2016, **1**, 371–377.

30 Y. Xu, B. Li, W. Li, J. Zhao, S. Sun and Y. Pang, *Chem. Commun.*, 2013, **49**, 4764–4766.

31 Z.-H. Fu, Y.-W. Wang and Y. Peng, *Chem. Commun.*, 2017, **53**, 10524–10527.

32 P. Das and S. K. Mandal, *J. Mater. Chem. C*, 2018, **6**, 3288–3297.

33 H. Ma, C. He, X. Li, O. Ablikim, S. Zhang and M. Zhang, *Sens. Actuators, B*, 2016, **230**, 746–752.

34 D. Samanta and P. S. Mukherjee, *Dalton Trans.*, 2013, **42**, 16784–16795.

35 K. Acharyya and P. S. Mukherjee, *Chem. Commun.*, 2014, **50**, 15788–15791.

36 S. Dalapati, S. Jin, J. Gao, Y. Xu, A. Nagai and D. Jiang, *J. Am. Chem. Soc.*, 2013, **135**, 17310–17313.

37 G. Lin, H. Ding, D. Yuan, B. Wang and C. Wang, *J. Am. Chem. Soc.*, 2016, **138**, 3302–3305.

38 G. Das, B. P. Biswal, S. Kandambeth, V. Venkatesh, G. Kaur, M. Addicoat, T. Heine, S. Verma and R. Banerjee, *Chem. Sci.*, 2015, **6**, 3931–3939.

39 D. Kaleeswaran and R. Murugavel, *J. Chem. Sci.*, 2018, **130**, 1–14.

40 (*a*) S. S. Nagarkar, B. Joarder, A. K. Chaudhari, S. Mukherjee and S. K. Ghosh, *Angew. Chem., Int. Ed.*, 2013, **52**, 2881–2885; (*b*) Y. Cui, Y. Yue, G. Qian and B. Chen, *Chem. Rev.*, 2012, **112**, 1126–1162; (*c*) B. Chen, S. Xiang and G. Qian, *Acc. Chem. Res.*, 2010, **43**, 1115–1124; (*d*) H. He, L. Hashemi, M.-L. Hu and A. Morsali, *Coord. Chem. Rev.*, 2018, **376**, 319–347; (*e*) A. Dutta, A. Singh, X. Wang, A. Kumar and J. Liu, *CrystEngComm*, 2020, **22**, 7736–7781; (*f*) M.-L. Hu, S. A. A. Razavi, M. Piroozzadeh and A. Morsali, *Inorg. Chem. Front.*, 2020, **7**, 1598–1632.

41 G. Chakraborty and S. K. Mandal, *Inorg. Chem.*, 2017, **56**, 14556–14566.

42 M. Bagheri, M. Y. Masoomi, A. Morsali and A. Schoedel, *ACS Appl. Mater. Interfaces*, 2016, **8**, 21472–21479.

43 X.-J. Hong, Q. Wei, Y.-P. Cai, S.-R. Zheng, Y. Yu, Y.-Z. Fan, X.-Y. Xu and L.-P. Si, *ACS Appl. Mater. Interfaces*, 2017, **9**, 4701–4708.

44 S. S. Dhankhar, N. Sharma, S. Kumar, T. J. D. Kumar and C. M. Nagaraja, *Chem. – Eur. J.*, 2017, **23**, 16204–16212.

45 S. S. Nagarkar, A. V. Desai and S. K. Ghosh, *Chem. Commun.*, 2014, **50**, 8915–8918.

46 P. Das and S. K. Mandal, *ACS Appl. Mater. Interfaces*, 2018, **10**, 25360–25371.

47 (*a*) B. Joarder, A. V. Desai, P. Samanta, S. Mukherjee and S. K. Ghosh, *Chem. – Eur. J.*, 2015, **21**, 965–969; (*b*) J.-H. Qin, B. Ma, X.-F. Liu, H.-L. Lu, X.-Y. Dong, S.-Q. Zang and H. Hou, *Dalton Trans.*, 2015, **44**, 14594–14603; (*c*) H.-R. Fu, L.-B. Yan, N.-T. Wu, L.-F. Ma and S.-Q. Zang, *J. Mater. Chem.*

A, 2018, **6**, 9183–9191; (*d*) Y. Rachuri, B. Parmar, K. K. Bisht and E. Suresh, *Dalton Trans.*, 2016, **45**, 7881–7892; (*e*) H.-R. Fu, Y. Zhao, T. Xie, M.-L. Han, L.-F. Ma and S.-Q. Zang, *J. Mater. Chem. C*, 2018, **6**, 6440–6448.

48 B. Wang, X.-L. Lv, D. Feng, L.-H. Xie, J. Zhang, M. Li, Y. Xie, J.-R. Li and H.-C. Zhou, *J. Am. Chem. Soc.*, 2016, **138**, 6204–6216.

49 (*a*) Y. Rachuri, B. Parmar, K. K. Bisht and E. Suresh, *Cryst. Growth Des.*, 2017, **17**, 1363–1372; (*b*) X.-X. Wu, H.-R. Fu, M.-L. Han, Z. Zhou and L.-F. Ma, *Cryst. Growth Des.*, 2017, **17**, 6041–6048; (*c*) J.-D. Xiao, L.-G. Qiu, F. Ke, Y.-P. Yuan, G.-S. Xu, Y.-M. Wang and X. Jiang, *J. Mater. Chem. A*, 2013, **1**, 8745–8752; (*d*) S. Shanmugaraju, C. Dabadie, K. Byrne, A. J. Savyasachi, D. Umadevi, W. Schmitt, J. A. Kitchen and T. Gunnlaugsson, *Chem. Sci.*, 2017, **8**, 1535–1546.

50 P. Das and S. K. Mandal, *J. Mater. Chem. A*, 2018, **6**, 16246–16256.

51 B. Parmar, Y. Rachuri, K. K. Bisht, R. Laiya and E. Suresh, *Inorg. Chem.*, 2017, **56**, 2627–2638.

52 K. Håkansson, R. V. Coorey, R. A. Zubarev, V. L. Talrose and P. J. Hakansson, *Mass Spectrom.*, 2000, **35**, 337–346.

53 J. M. Sylvia, J. A. Janni, J. D. Klein and K. M. Spencer, *Anal. Chem.*, 2000, **72**, 5834–5840.

54 V. P. Anferov, G. V. Mozjoukhine and R. Fisher, *Rev. Sci. Instrum.*, 2000, **71**, 1656–1659.

55 D. S. Moore, *Rev. Sci. Instrum.*, 2004, **75**, 2499–2512.

56 K. M. Roscioli, E. Davis, W. F. Siems, A. Mariano, W. Su, S. K. Guharay and H. H. Hill, Jr., *Anal. Chem.*, 2011, **83**, 5965–5971.

57 J. C. Chen, J. L. Shih, C. H. Liu, M. Y. Kuo and J. M. Zen, *Anal. Chem.*, 2006, **78**, 3752–3757.

58 I. A. Popov, H. Chen, O. N. Kharybin, E. N. Nikolaev and R. G. Cooks, *Chem. Commun.*, 2005, 1953–1955.

59 R. D. Luggar, M. J. Farquharson, J. A. Horrocks and R. J. Lacey, *X-Ray Spectrum.*, 1998, **27**, 87–94.

60 L. He, B. Dong, Y. Liu and W. Lin, *Chem. Soc. Rev.*, 2016, **45**, 6449–6461.

61 H. Chen, B. Dong, Y. Tang and W. Lin, *Acc. Chem. Res.*, 2017, **50**, 1410–1422.

62 G. Chakraborty and S. K. Mandal, *ACS Omega*, 2018, **3**, 3248–3256.

63 I. Ravikumar and P. Ghosh, *Inorg. Chem.*, 2011, **50**, 4229–4231.

64 (*a*) Y. Mikata, A. Yamashita, A. Kawamura, H. Konno, Y. Miyamoto and S. Tamotsu, *Dalton Trans.*, 2009, 3800–3806; (*b*) Y. Mikata, Y. Sato, S. Takeuchi, Y. Kuroda, H. Konno and S. Iwatsuki, *Dalton Trans.*, 2013, **42**, 9688–9698; (*c*) Y. Mikata, Y. Nodomi, A. Kizu and H. Konno, *Dalton Trans.*, 2014, **43**, 1684–1690; (*d*) Y. Mikata, S. Takeuchi, E. Higuchi, A. Ochi, H. Konno, K. Yanaid and S.-I. Sato, *Dalton Trans.*, 2014, **43**, 16377–16386; (*e*) Y. Mikata, A. Kizu, K. Nozaki, H. Konno, H. Ono, S. Mizutani and S.-I. Sato, *Inorg. Chem.*, 2017, **56**, 7404–7415; (*f*) R. Montis, M. C. Aragoni, M. Arca, C. Bazzicalupi, A. J. Blake, C. Caltagirone, G. D. Filippo, A. Garau, P. Gratteri, F. Isaia, V. Lippolis and A. Pintus,

Inorg. Chim. Acta, 2012, **381**, 170–180; (*g*) V. Amendola, C. Mangano and P. Pallavicini, *Dalton Trans.*, 2004, 2850–2854; (*h*) Y. Mikata, M. Wakamatsu and S. Yano, *Dalton Trans.*, 2005, 545–550.

65 Y. Dong, R. Fan, W. Chen, P. Wang and Y. Yang, *Dalton Trans.*, 2017, **46**, 6769–6775.

66 (*a*) L. Xue, H.-H. Wang, X.-J. Wang and H. Jiang, *Inorg. Chem.*, 2008, **47**, 4310–4318; (*b*) Y. Dai, X. Liu, P. Wang, J. Fu, K. Yao and K. Xu, *RSC Adv.*, 2016, **6**, 99933–99939.

67 B. Zhang, H. Liu, F. Wu, G. Hao, Y. Chen, C. Tan, Y. Tan and Y. Jiang, *Sens. Actuators, B*, 2017, **243**, 765–774.

68 (*a*) M. Sohrabi, M. Amirnasr, H. Farrokhpour and S. Meghdadi, *Sens. Actuators, B*, 2017, **250**, 647–658; (*b*) M. Sohrabi, M. Amirnasr, S. Meghdadi, M. Lutz, M. B. Torbati and H. Farrokhpour, *New J. Chem.*, 2018, **42**, 12595–12606.

69 (*a*) J. M. Jung, J. H. Kang, J. Han, H. Lee, M. H. Lim, K.-T. Kim and C. Kim, *Sens. Actuators, B*, 2018, **267**, 58–69; (*b*) S. Sinha, B. Chowdhury, N. N. Adarsh and P. Ghosh, *Dalton Trans.*, 2018, **47**, 6819–6830; (*c*) S. J. Ranee, G. Sivaraman, A. M. Pushpalatha and S. Muthusubramanian, *Sens. Actuators, B*, 2018, **255**, 630–637.

70 (*a*) S. K. Asthana, A. Kumar, S. K. Hira, P. P. Manna and K. K. Upadhyay, *Inorg. Chem.*, 2017, **56**, 3315–3323; (*b*) S. Halder, P. Ghosh, A. Hazra, P. Banerjee and P. Roy, *New J. Chem.*, 2018, **42**, 8408–8414.

71 K. S. Asha, K. Bhattacharyya and S. Mandal, *J. Mater. Chem. C*, 2014, **2**, 10073–10081.

72 J. R. Lakowicz, *Principles of Fluorescence Spectroscopy*, Springer, New York, USA, 2006.

73 (*a*) L.-H. Zeng, C. Wang, T. Wang and D.-L. Li, *Analyst*, 2016, **141**, 5339–5345; (*b*) N. Shao, Y. Zhang, S. Cheung, R. Yang, W. Chan, T. Mo, K. Li and F. Liu, *Anal. Chem.*, 2005, **77**, 7294–7303; (*c*) A. Credi and L. Prodi, *J. Mol. Struct.*, 2014, **1077**, 30–39; (*d*) A. Credi and L. Prodi, *Spectrochim. Acta, Part A*, 1998, **54**, 159–170; (*e*) A. V. Fonin, A. I. Sulatskaya, I. M. Kuznetsova and K. K. Turoverov, *PLoS One*, 2014, **9**, e103878.

74 (*a*) A. Abbasi and M. Shakir, *New J. Chem.*, 2018, **42**, 293–300; (*b*) S. Chen, Y.-L. Yu and J.-H. Wang, *Anal. Chim. Acta*, 2018, **999**, 13–26; (*c*) N. Jiang, G. Li, W. Che, D. Zhu, Z. Su and M. R. Bryce, *J. Mater. Chem. C*, 2018, **6**, 11287–11291.

75 M. J. Frisch, G. W. Trucks, H. B. Schlegel, G. E. Scuseria, M. A. Robb, J. R. Cheeseman, G. Scalmani, V. Barone, B. Mennucci, G. A. Petersson, H. Nakatsuji, M. Caricato, X. Li, H. P. Hratchian, A. F. Izmaylov, J. Bloino, G. Zheng, J. L. Sonnenberg, M. Hada, M. Ehara, K. Toyota, R. Fukuda, J. Ishida, M. Hasegawa, T. Nakajima, Y. Honda, O. Kitao, H. Nakai, T. Vreven, J. A. Montgomery, J. E. Peralta, F. Ogliaro, M. Bearpark, J. J. Heyd, E. Brothers, K. N. Kudin, V. N. Staroverov, T. Keith, R. Kobayashi, J. Normand, K. Raghavachari, A. Rendell, J. C. Burant, S. S. Iyengar, J. Tomasi, M. Cossi, N. Rega, J. M. Millam, M. Klene, J. E. Knox, J. B. Cross, V. Bakken, C. Adamo, J. Jaramillo, R. Gomperts, R. E. Stratmann, O. Yazyev, A. J. Austin, R. Cammi, C. Pomelli, J. W. Ochterski, R. L. Martin, K. Morokuma, V. G. Zakrzewski, G. A. Voth, P. Salvador, J. J. Dannenberg, S. Dapprich, A. D. Daniels, O. Farkas, J. B. Foresman, J. V. Ortiz, J. Cioslowski and D. J. Fox, *Gaussian 09*, Gaussian, Inc., Wallingford, CT, 2013.

76 Accelrys, *Materials Studio Getting Started, release 5.0*, Accelrys Software, Inc., San Diego, CA, 2009.

77 (*a*) X. Cao, N. Zhao, H. Lv, Q. Ding, A. Gao, Q. Jing and T. Yi, *Langmuir*, 2017, **33**, 7788–7798; (*b*) A. K. Bandela, S. Bandaru and C. P. Rao, *Chem. – Eur. J.*, 2015, **21**, 13364–13374.